Inorganic Chemistry

Article

pubs.acs.org/IC

Copper(II)-Binding Ability of Stereoisomeric *cis*- and *trans*-2-Aminocyclohexanecarboxylic Acid–L-Phenylalanine Dipeptides. A Combined CW/Pulsed EPR and DFT Study

Nóra V. Nagy,*[,†] Sabine Van Doorslaer,[‡] Terézia Szabó-Plánka,[§] Senne Van Rompaey,[‡] Andrea Hamza,[†] Ferenc Fülöp,[∥] Gábor K. Tóth,[⊥] and Antal Rockenbauer[†]

[†]Institute of Structural Chemistry, Chemical Research Center of the Hungarian Academy of Sciences, Pusztaszeri út 59-67, H-1025 Budapest, Hungary

[‡]Department of Physics, University of Antwerp, B-2610 Wilrijk-Antwerp, Belgium

[§]Department of Physical Chemistry and Materials Sciences, University of Szeged, Aradi vértanúk tere 1, H-6720 Szeged, Hungary

[∥]Institute of Pharmaceutical Chemistry, University of Szeged, Eötvös u. 6, H-6720 Szeged, Hungary

[⊥]Faculty of Medicine, University of Szeged, Dóm tér 8, H-6720 Szeged, Hungary

Supporting Information

ABSTRACT: With the aim of an improved understanding of the metal-complexation properties of alicyclic β-amino acid stereoisomers, and their peptides, the complex equilibria and modes of coordination with copper(II) of L-phenylalanine (F) derivatives of *cis*/*trans*-2-aminocyclohexanecarboxylic acid (*c*/*t*ACHC), *i.e.* the dipeptides F-*c*/*t*ACHC and *c*/*t*ACHC-F, were investigated by a combination of CW and pulsed EPR methods. For the interpretation of the experimental data, DFT quantum-chemical calculations were carried out. Simulation of a pH-dependent series of room-temperature CW-EPR spectra revealed the presence of EPR-active complexes ($[Cu(aqua)]^{2+}$, $[CuL]^{+}$, $[CuLH_{-1}]$, $[CuLH_{-2}]^{-}$, and $[CuL_2H_{-1}]^{-}$), and an EPR-inactive species ($[Cu_2L_2H_{-3}]^{-}$) in aqueous solutions for all studied cases. $[CuLH]^{2+}$ was included in the equilibrium model for the *c*/*t*ACHC-F–copper(II) systems, and $[CuL_2]$, together with two coordination isomers of $[CuL_2H_{-1}]^{-}$, were also identified in the F-*t*ACHC–copper(II) system. Comparison of the complexation properties of the diastereomeric ligand pair F-(1*S*,2*R*)-ACHC and F-(1*R*,2*S*)-ACHC did not reveal significant differences. Considerably lower formation constants were obtained for the *trans* than for the *cis* isomers for both the F-*c*/*t*ACHC and the *c*/*t*ACHC-F pairs in the case of $[CuLH_{-1}]$ involving tridentate coordination by the amino, the deprotonated peptide, and the carboxylate groups. A detailed structural analysis by pulsed EPR methods and DFT calculations indicated that there was no significant destabilization for the complexes of the *trans* isomers. The lower stability of their complexes was explained by the limitation that only the conformer with donor groups in equatorial–equatorial ring positions can bind to copper(II), whereas both equatorial-axial conformers of the *cis* isomers are capable of binding. From a consideration of the proton couplings obtained with X-band ^{1}H HYSCORE, ^{2}H exchange experiments, and DFT, the thermodynamically most stable cyclohexane ring conformer was assigned for all four $[CuLH_{-1}]$ complexes. For the F-*cA*CHC case, the conformer did not match the most stable conformer of the free ligand.

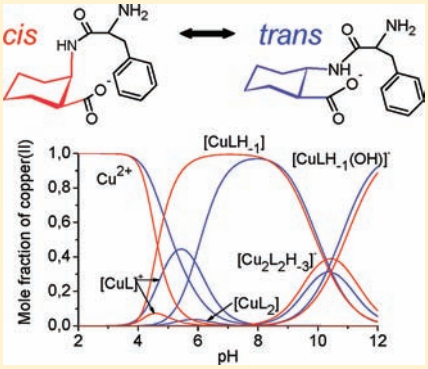

INTRODUCTION

The recent increase in interest in alicyclic β-amino acids and their derivatives has been stimulated by their biological activity and natural occurrence. The most widely investigated cyclic β-amino acid is the (1*R*,2*S*)-2-aminocyclopentanecarboxylic acid (*cispentacin*, ACPC), which has been isolated from *Bacillus cereus* and *Streptomyces setonii* and is used in the antibiotic amipurimycin.[1] Its L-phenylalanine derivative also exhibits excellent antifungal activity against *Candida albicans*.[2] The β-amino acids can be used as building blocks for the preparation of modified (unnatural) analogues of biologically active peptides. Through replacement of an α-amino acid by a β-amino acid, the conformational stability and the resistance to enzymatic degradation can be enhanced.[1,3] Some oligopeptides built up from β-amino acids have been found to fold into stable helical structures.[4−6] Cyclopentanecarboxylic acid derivatives of such helices have proven to be promising antimicrobial drug candidates.[6] By modulating the secondary structure of the peptides, their function can be altered, which opens the way to targeted drug design. The cyclic β-amino acid residues play a very important role in controlling peptide folding.[7−10] β-Peptides with helical structures can interact with

Received: July 27, 2011
Published: January 6, 2012

   dx.doi.org/10.1021/ic2016116 | *Inorg. Chem.* 2012, 51, 1386−1399

special macromolecular targets. For example, a helical β-peptide has been reported to inhibit the interaction between the transcription factor that controls the cell fate in response to stress (p53) and the human oncogene product double minute 2 (hDM2), which is an important goal in cancer therapy.[11] Peptides containing β-amino acids, such as ACPC and 2-aminocyclohexanecarboxylic acid (ACHC), have been recently investigated as potential antimicrobial agents and showed potent antibacterial[12] and antifungal[13] activity. The amphiphilicity of the oligomers formed from these β-peptides has an appreciable impact on the antibacterial effect. Furthermore, the flexibility and hydrophilic/lipophilic balance of the backbone are necessary for considerable antimicrobial activity.[14] Computer simulations of the adsorption of such amphiphilic molecules to the lipid membrane have revealed a correlation between the membrane-binding properties (penetration depth) and the observed antimicrobial activity, suggesting that efficient binding is necessary for the biological activity.[15] For the latter studies, β-phenylalanine has been used as hydrophobic residue.

Although the coordination of transition-metal ions (e.g., Zn^{2+} or Cu^{2+}, which are present in relatively high concentrations in biological systems) can often significantly modify the biological effects or secondary structures of cyclic β-amino acids,[16] relatively little information is available on their metal-binding ability. To our knowledge, their complexation properties have only been considered in the context of distinguishing the enantiomers of β-amino acids by means of mass spectrometry.[17] The complexation properties of different stereochemical and conformational isomers of disubstituted cyclohexanes have likewise barely been studied, though the stereochemistry frequently is expected to have a huge impact on the biological activity. 1,2-Disubstituted cyclohexane derivatives of tripeptide aldehydes, for example, inhibit thrombin,[18] whereby the derivatives with *cis* stereochemistry display high inhibitor activity, while the *trans* complexes exhibit only a weak effect.[19] Since the coordination of short peptides is very important, we set out to study the dipeptide derivatives of disubstituted cyclohexanes. L-Phenylalanine (F) was chosen as the other amino acid because of its prospective biological activity. Furthermore, the results may reflect the behavior of other amino acids with a noncoordinating side-chain. In the present work, we report on an investigation of the copper(II)-binding abilities of four dipeptides formed from F and *cis*- or *trans*-2-aminocyclohexanecarboxylic acid (*c*ACHC and *t*ACHC, respectively): F-*c*ACHC, F-*t*ACHC, *c*ACHC-F, and *t*ACHC-F (Figure 1). The effects of the *trans* and *cis* stereochemistry and of the C- or N-terminal position of the β-amino acids on the Cu(II) complexation are compared.

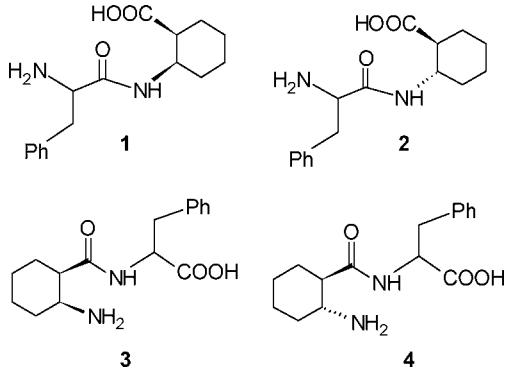

Figure 1. Structures of the ligands (LH): **1**, F-*c*ACHC; **2**, F-*t*ACHC; **3**, *c*ACHC-F; **4**, *t*ACHC-F.

In the following, we first analyze the free dipeptide ligands. We report on the conformational properties of the cyclohexane ring investigated by means of density functional theory (DFT) calculations, and the protonation constants of the free ligands determined by pH-potentiometry. In the next section, the structures and constitutions of the copper(II) complexes formed in aqueous solution were characterized by room-temperature X-band continuous-wave electron paramagnetic resonance (CW-EPR) experiments. Further structural information on the prevailing *mono*complexes was gained from the combination of low-temperature X-band CW and W-band electron spin echo (ESE)-detected EPR spectra, which allowed determination of the anisotropic *g* and copper and nitrogen hyperfine constants. Furthermore, W-band electron electron double resonance (ELDOR)-detected NMR experiments were performed in order to obtain more precise data on the coordinated nitrogen hyperfine and nuclear quadrupole tensors, which contribute to the simulation of the CW-EPR data. In turn, X-band hyperfine sublevel correlation (^{1}H-HYSCORE) spectroscopic measurements were applied to obtain the ligand proton hyperfine tensors, which reflect the steric position of the noncoordinating part of the ligand. In order to corroborate the interpretation of the experimental results, DFT calculations were also carried out.

MATERIALS AND METHODS

Materials. The amino acids *c*ACHC and *t*ACHC were prepared as described previously.[1] In the peptide syntheses, L-phenylalanine (F) from Sigma-Aldrich and racemic mixtures of the enantiomers (1*S*,2*R*)-ACHC and (1*R*,2*S*)-ACHC for *cis*-ACHC, and (1*R*,2*R*)-ACHC and (1*S*,2*S*)-ACHC for *trans*-ACHC were used, and mixtures of diastereomers were obtained. Dipeptides were synthesized in the liquid phase by using *tert*-butyloxycarbonyl (^{t}Boc) methodology. The diastereomers formed in the syntheses were separated by HPLC on a Lichrosorb 10RP18/100 semipreparative column. The purities of the products were measured by HPLC, ESI-MS, and NMR techniques. For determination of the absolute configurations of the diastereomers, the amide bond was split, and the retention time of the β-amino acid obtained was compared with that of an β-amino acid standard, using a HPLC technique. The neutral form of a ligand is denoted as LH.

Methods. pH-potentiometric titrations for determination of the protonation constants of the dipeptides were carried out in aqueous solution (I = 0.2 M NaCl, T = 298 K) under an argon atmosphere, through the use of an automatic Dosimat autoburet combined with a Radiometer PHM240 pH/ion meter. The pH was adjusted with NaOH solution and measured with a Methrom 6.0234.100 glass electrode, which was calibrated with IUPAC standard buffers from Radiometer. The protonation constants were determined from three independent titrations with a dipeptide concentration of 4 mM. Data were evaluated with the PSEQUAD computer program.[20]

All CW-EPR spectra were recorded with a BRUKER EleXsys E500 spectrometer (microwave frequency 9.81 GHz, microwave power 10 mW, modulation amplitude 5 G, modulation frequency 100 kHz). During a titration, the isotropic EPR spectra were recorded at 298 K in a circulating system. For each system, two titrations were carried out under an argon atmosphere: one at equal copper(II) chloride and ligand concentrations (3 mM), and another at 1 mM copper(II) chloride and 10−15 mM ligand. NaOH solution was used to change the pH, which was measured with a Radiometer PHM240 pH/ion meter equipped with a Metrohm 6.0234.100 glass elecrode. A Heidolph Pumpdrive 5101 peristaltic pump was used to circulate the solution from the titration pot through a capillary tube into the cavity of the instrument. 19−24 spectra were recorded in the pH range 2−12.5.

dx.doi.org/10.1021/ic2016116 | *Inorg. Chem.* 2012, 51, 1386−1399

At various pH values, where predominant species were formed, samples of 100 μL were taken, and 30 μL of methanol was added to avoid crystallization during freezing. The samples were then frozen in liquid nitrogen, and the CW-EPR spectra were recorded under the same instrumental conditions as the room-temperature spectra described above.

ESE-detected EPR and ELDOR-detected NMR measurements[21] were carried out with a W-band (95 GHz) Bruker ELEXSYS E680 spectrometer in conjunction with a split-coil Oxford 6T superconducting magnet equipped with an Oxford flow cryostat and a Bruker cylindrical cavity at 6 K. For the latter measurements, the pulse sequence was $HTA_{mw2}-T-\pi/2_{mw1}-\tau-\pi_{mw1}-\tau-$echo sequence, with the length of the high-turning angle (HTA) pulse 22 μs, $t_{\pi/2}$ = 240 ns, and t_π = 480 ns. Delay times of T = 4.4 μs and τ = 848 ns were applied. Spectra were recorded at 7−8 different observer positions, with 20−45 scans for each spectrum depending on the echo intensity.

The HYSCORE[22] spectra were measured at X-band microwave frequencies with a Bruker ESP380E spectrometer (9.76 GHz) equipped with a liquid He cryostat from Oxford, Inc. A pulse sequence of $\pi/2-\tau-\pi/2-t_1-\pi-t_2-\pi/2-\tau-$echo, with pulse lengths $t_{\pi/2} = t_\pi$ = 16 ns was applied. Three τ values (96, 176, and 248 ns) were used to avoid blind spots, and the corresponding spectra were added together in the frequency domain after normalization to the noise level to avoid blind spots. An eight-step phase cycle was utilized to eliminate unwanted echoes. The aqueous solution samples containing 3 mM copper(II) and 3 mM ligand at pH ∼ 7.5−8.2 were measured at 10 K, at three different observer positions ($g \approx g_x$, B_0 = 334.0 mT; intermediate position, B_0 = 320.0 mT, and $g = g_z$, $M_I = {}^3/_2$, B_0 = 284.0 mT). Subsequently, the measurements were repeated with samples containing 1 mM copper(II) and 1 mM ligand at the same pH values, in a 60% vol/vol D_2O/H_2O solution mixture, in order to eliminate the signals of exchangeable (amino and water) protons.

Evaluation of EPR Spectra. The series of room-temperature CW-EPR spectra were simulated simultaneously by a "two-dimensional" method using the 2D_EPR program.[23] Each component curve was described by the isotropic EPR parameters g_o, the copper hyperfine (A_o^{Cu}) and nitrogen hyperfine (A_o^N) couplings, and the relaxation parameters a, b, and c, which define the line widths in the equation $\sigma_{MI} = a + bM_I + cM_I^2$, where M_I is the magnetic quantum number of the copper nucleus. The concentrations of the complexes were varied by fitting their formation constants, defined by the following general equilibrium:

$$pM + qH + rL \rightleftharpoons M_pH_qL_r$$

$$\beta_{M_pH_qL_r} = \frac{[M_pH_qL_r]}{[M]^p[H]^q[L]^r}$$

where M denotes the metal ion and L the nonprotonated ligand molecule. For each spectrum, the noise-corrected regression parameter (R_j for the jth spectrum) is derived from the average square deviation (SQD) between the experimental and the calculated intensities. For the series of spectra, the fit is characterized by the overall regression coefficient R, calculated from the overall average SQD. The details of the statistical analysis were published previously.[23] The R values obtained for the best simulation of the spectra were 0.9944, 0.9957, 0.9904, and 0.9924 for the F-*c*ACHC−, F-*t*ACHC−, *c*ACHC-F−, and *t*ACHC-F−copper(II) equilibrium systems, respectively. For the determination of the formation constants of EPR-inactive complexes, the difference between the analytical and calculated total copper(II) concentrations was minimized.

The anisotropic spectra were analyzed individually with the EPR program,[24] which gives the anisotropic EPR parameters (g_x, g_y, g_z, A_x^{Cu}, A_y^{Cu}, A_z^{Cu}, A_x^N, A_y^N, and A_z^N) and the orientation-dependent line width parameters. For each system, two EPR spectra recorded at 77 K were selected and simulated, for which the predominant complexes [$CuLH_{-1}$] or [$CuLH_{-1}(OH)$]$^-$ were formed. Since a natural copper(II) chloride was used for the measurements, the spectra were calculated as the sum of the spectra of ^{63}Cu and ^{65}Cu weighted by their natural abundances. The quality of the fit was characterized by the noise-corrected regression parameter R_j as above. The copper and nitrogen coupling constants and the relaxation parameters were obtained in field units and then converted to MHz, using the standard equation A [MHz] = 28.024944(g/g_e)A [mT].

All pulsed-EPR (ESE-detected EPR, ELDOR-detected NMR and HYSCORE) spectra were simulated by using the EasySpin program package.[25] For simulation of the ELDOR-detected NMR spectra, the ENDOR-simulation functions were used, and the nuclear hyperfine and quadrupole couplings of two strongly coupled nitrogens were taken into account.

The HYSCORE data were processed with MATLAB (MathWorks, Inc., Natick, MA). The time traces of the HYSCORE spectra were baseline-corrected with a third-order polynomial, apodized with a Hamming window and zero-filled. After a two-dimensional Fourier transformation, the absolute-value spectra were calculated.

Theoretical Computations. DFT computations were performed with the Gaussian program[26] for the conformational study of the free ligands in vacuum, in aqueous solution at 298 K, and in aqueous solution at 77 K. The calculations were done at the B3LYP/6-31G* level of theory and, with application of the default polarizable continuum model (PCM) in the event of the presence of solvent. Geometry optimization was carried out for the two chair conformers. The effect of the phenyl ring position relative to the ligand was then examined. In the next step, the distribution (percentages) of the different ligand structures was calculated from their Gibbs free energies at room temperature and at 77 K. Thereafter, the structures relating to the same chair conformations were summed to obtain the final ratio of the two chair conformers.

For the copper complexes of selected ligand conformations, spin-unrestricted DFT computations were performed with the ORCA package.[27−31] To simulate the solvent, the conductor-like screening model[32] (COSMO) was applied with the dielectric constant of water. For the geometry optimizations, the B3LYP functional was used. The split-valence pulse polarization (SV(P)) basis set[33] was used for all atoms except copper, for which a more polarized triple-ζ valence (TZVPP) basis[33] was chosen.

In the next step, single-point calculations for the optimized geometries were carried out to predict the EPR and NMR spectral parameters. In these calculations, the B3LYP functional[34] was taken, and the triply polarized "core properties" (CP(PPP)) basis set[35] was used for the copper atom, the SVP basis set for the carbon and oxygen atoms, and the Barone "EPR-II" basis set[36] for the nitrogen and hydrogen atoms.

RESULTS AND DISCUSSION

Analysis of the Free Dipeptides under Study. *DFT Analysis of the Free Ligand Stereochemistry.* The stereochemistry of the investigated dipeptides is rather complex. The different donor-group positions may result in slightly different structures for the final copper(II) complexes. For this reason, the distribution of the different conformers of the free ligands (L) was calculated by DFT computation. First of all, we took into consideration that, in each dipeptide synthesis, two diastereomers were formed from the chiral F and the racemic mixture of the two enantiomers of *cis*-ACHC ((1*S*,2*R*)-ACHC and (1*R*,2*S*)-ACHC) or *trans*-ACHC ((1*S*,2*S*)-ACHC and (1*R*,2*R*)-ACHC). Additionally, the cyclohexane ring can flip-flop in aqueous solution at room temperature, and hence, different ring conformers may coexist. The variety of structures with the different diastereomers and chair conformers are schematically illustrated for F-*c*ACHC in Figure 2. Geometry optimization was carried out for the two chair conformers of one diastereomer. In conformer (1), an axial (a) carboxylate group and an equatorial (e) amide group were assumed, while

dx.doi.org/10.1021/ic2016116 | Inorg. Chem. 2012, 51, 1386−1399

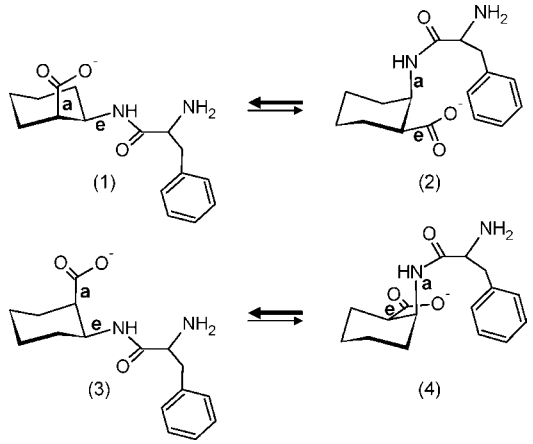

Figure 2. Structures of F-*c*ACHC isomer. (1) and (2) are the chair conformers of the diastereoisomer F-(1*S*,2*R*)-ACHC, and (3) and (4) are the conformers for F-(1*R*,2*S*)-ACHC.

the positions of the donor groups were the reverse for conformer (2) (Figure 2). The percentages of the two types of chair conformers obtained by conformational analysis are presented in Table 1.

Table 1. Free Ligand Conformer Ratios Calculated by DFT[a]

ligand	conformer	conformer % at 298 K	conformer % at 77 K
F-*c*ACHC	conf 1: $a_{carb} - e_{amide}$	92.2	100.0
	conf 2: $e_{carb} - a_{amide}$	7.8	0.0
F-*t*ACHC	conf 1: $e_{carb} - e_{amide}$	99.9	100.0
	conf 2: $a_{carb} - a_{amide}$	0.1	0.0
*c*ACHC-F	conf 1: $a_{am} - e_{amide}$	74.2	79.5
	conf 2: $e_{am} - a_{amide}$	25.8	20.5
*t*ACHC-F	conf 1: $e_{am} - e_{amide}$	100.0	100.0
	conf 2: $a_{am} - a_{amide}$	0.0	0.0

[a]Abbreviations: a, axial position; e, equatorial position; carb, carboxylate group; amide, amide group; am, amino group.

To interpret these results, comparison with the conformational studies of 1-substituted cyclohexanes[37] may be useful. In the latter study, it was pointed out that steric and electrostatic repulsion occur between the axial bulky group and the axial H-3 and H-5, making the axial position of the bulky group unfavored. In agreement with expectation, our results indicated that conformer (1), with both 1,2-substituents equatorial, accounts for almost 100% of the *trans* isomers (see Figure S1 in the Supporting Information). In F-*c*ACHC, the prevalence of the conformer in which the peptide bond is equatorial and the carboxylate group is axial is 92.2% (structures (1) and (3) in Figure 2). The other chair conformer is highly unfavored (structure (2) and (4) in Figure 2). In *c*ACHC-F, conformer (1) with the amide group equatorial is strongly preferred, though conformer (2) is also formed in a significant amount (25.8%). The different distributions for F-*c*ACHC and *c*ACHC-F can be attributed to the charge differences between their second bulky groups: the negatively charged COO^- group in F-*c*ACHC probably has a much stronger axial preference as compared with the NH_2 group in *c*ACHC-F. The distribution of the different conformers at 77 K was also calculated. The predominance of the more stable conformer (1) was either preserved or further increased (Table 1). To summarize, this analysis predicts the predominance of one of the conformers of the free ligands in aqueous solutions. It should be noted, however, that this does not necessarily hold for complex formation, as will be shown later.

Deprotonation Constants for the Free Ligands. The deprotonation constants of the free ligands, determined by pH-potentiometry, are presented in Table 2 together with literature data on glycyl-β-alanine (Gly-β-Ala) and β-alanyl-glycine (β-Ala-Gly).[38] It can be concluded that the deprotonation pK values of the groups located in the phenylalanine part of the ligands are very similar for the *cis*/*trans* ligand pairs: ΔpK(COOH) = 0.02 for *c*/*t*ACHC-F and $\Delta\beta$(LH) = 0.1 for F-*c*/*t*ACHC. At the same time, the differences are larger when the donor group is situated in the cyclohexane ring: ΔpK(COOH) = 0.23 for F-*c*/*t*ACHC and $\Delta\beta$(LH) = 0.35 for the amino deprotonation in *c*/*t*ACHC-F. This suggests small differences in electrostatic distribution between the *cis* and *trans* stereoisomers. In the *cis* ligands, the carboxylate and amino groups are slightly more basic. The difference is larger when the N- or C-terminal positions of the β-amino acids are compared. Similarly to β-Ala-Gly, *c*/*t*ACHC-F has more basic amino groups (higher value of log β_{LH}) and more acidic carboxylate groups (lower pK(COOH)) as compared with Gly-β-Ala and F-*c*/*t*ACHC, respectively (Table 2). The difference between the ACHC dipeptide pairs is higher, as a consequence of the positive inductive effect of the phenyl group. From these results, high similarities for the complexation properties of the *cis*−*trans* isomers of the ligands may be expected.

Analysis of the Cu(II) Complexation of the Dipeptides under Study. *General.* The complexation properties of diastereomer and conformer peptides are now compared using different EPR techniques. The coordination of diastereomeric peptide ligands to copper(II) was investigated by Sóvágó et al. by pH-potentiometric, spectrophotometric, CD, and EPR methods, but no significant stereoselectivity was observed.[39] Similarly, the crystal structures of the racemic dipeptides Cu(Gly-D-Val) and Cu(Gly-L-Val) were found to be almost in complete agreement (except for the configuration around the asymmetric carbon atom).[40] We therefore first check whether the EPR spectra of the copper(II) complexes of two diastereomers of the dipeptides under study differ significantly. We restrict here the discussion to the F-*c*ACHC case.

In the present work, a titration was performed in the presence of copper(II) for both the racemic mixture of the ligand and the separated diastereomers F-(1*S*,2*R*)-2-ACHC and F-(1*R*,2*S*)-2-ACHC, and room-temperature CW-EPR spectra (not shown) and low-temperature CW-EPR spectra (Figure 3) were recorded. The evaluation of the spectral series revealed that the copper(II) complexes of the diastereomers cannot be distinguished: both their EPR spectra and formation constants agree within experimental error. DFT calculations were also carried out on the two diastereomers of the above complexes, and no significant differences (i.e., differences larger than the experimental error) could be revealed for the theoretically calculated EPR data (see Supporting Information, Table S1).

Since the physical−chemical parameters of diastereomeric ligands can differ significantly, the above results might appear unexpected at first glance. However, the similarities between the Cu(II) complexes can be understood by a closer consideration of the ligand structure. Figure 2 shows that the orientation of the donor groups is the same for the corresponding conformations, (1) and (3), of the two diastereomers, resulting in similar local environments around the copper(II) and, hence, very similar EPR parameters. The same holds for structures (2) and (4) and

dx.doi.org/10.1021/ic2016116 | *Inorg. Chem.* 2012, 51, 1386−1399

Table 2. Formation Constants as log β Determined with the 2D Simulation Procedure of the Isotropic EPR Spectra for the Copper(II) Complexes of F-*c*/*t*ACHC and *c*/*t*ACHC-F[a], along with the Deprotonation Constants of the Free Ligands

complex	F-*c*ACHC	F-*t*ACHC	*c*ACHC-F	*t*ACHC-F	Gly-β-Ala[b]	β-Ala-Gly[b]
Deprotonation Constants						
LH_2[c]	12.02(1)	11.89(1)	12.32(1)	11.94(1)	12.13	12.64
LH[c]	7.45(1)	7.55(1)	9.09(1)	8.74(1)	8.12	9.48
p*K*(COOH)	4.57	4.34	3.23	3.21	4.01	3.16
Formation Constants						
$[CuLH]^{2+}$			11.01(1)	10.09(1)	9.71	10.64
$[CuL]^{+}$	5.13(1)	5.24(1)	5.64(2)	3.92(3)	5.69	5.99
$[CuLH_{-1}]$	1.29(1)	−0.63(1)	1.79(1)	−0.40(1)	0.91	1.21
$[CuLH_{-1}(OH)]^{-}$	−9.13(1)	−11.00(2)	−7.79(1)	−9.98(1)	−9.37	−8.90
$[CuL_2]$		9.22(2)				
$[CuL_2H_{-1}]^{-}$	3.27(3)	1.83[d]	4.12(1)	2.02(1)	3.38	3.81
isomer 1		1.26(2)				
isomer 2		1.56(3)				
$[Cu_2L_2H_{-3}]^{-}$	−4.4(5)	−5.0(4)	−5.0(6)	−6.1(7)		
p*K*(N_{amide})	3.84	5.87	3.85	4.32	4.78	4.78
p*K*(OH^{-})	10.42	10.37	9.58	9.58	10.28	10.11
log *K*[e]	1.98	2.46	2.33	2.42	2.47	2.60

[a]The confidence intervals of the last digit are given in parentheses. [b]Data from ref 38. [c]The formation constants of the proton complexes were measured by pH-potentiometry and fixed through the EPR simulation. [d]The overall log β = log($\beta_{isomer\ 1}$ + $\beta_{isomer\ 2}$). [e]log *K* = log $\beta(CuL_2H_{-1})$ − log $\beta(CuLH_{-1})$.

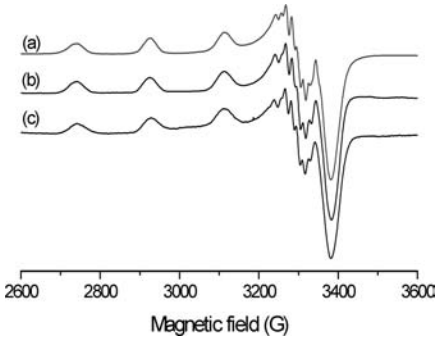

Figure 3. (a) Simulated X-band CW-EPR spectrum of $[CuLH_{-1}]$ for the ligand F-*c*ACHC, obtained with the parameters in Table 3, and (b, c) experimental spectra recorded in equimolar solutions of (b) F-(1*S*,2*R*)-ACHC, pH = 8.61 and (c) F-(1*R*,2*S*)-ACHC, pH = 8.01.

for the stereoisomers of F-*t*ACHC (Figure S1). Therefore, in the cases of the other three ligands (F-*t*ACHC, *c*ACHC-F, and *t*ACHC-F), only one of the two diastereomers was investigated: the coordination properties of the (1*S*,2*R*) diastereomers for the *cis* ligands and of the (1*S*,2*S*) diastereomers for the *trans* ligands. Accordingly, in the rest of the manuscript, the type of the diastereomer is omitted from the symbols of the ligands.

The next sections will focus on the study of the pH-dependent complex equilibria using room-temperature CW-EPR. Furthermore, since our DFT study of the free ligands showed that different conformers may exist for one diastereomer, a combination of low-temperature CW-EPR, pulsed EPR, and DFT is used to investigate whether the dominant conformer of the free dipeptide is retained upon copper(II) complexation.

Room-Temperature CW-EPR Experiments. *Equilibrium Model.* The EPR parameters and formation constants were determined by the simultaneous "two-dimensional" analysis of series of room-temperature EPR spectra (Figure 4 and Figures S2−S4). The protonation constants obtained for the free ligands by pH-potentiometry were used without further fitting in this model. The formation constants for the copper(II) complexes are listed in Table 2, while the distributions of copper(II) among the various complexes, calculated from these equilibrium constants, are depicted in Figure 5. The EPR-active complexes $[Cu(aqua)]^{2+}$, $[CuL]^{+}$, $[CuLH_{-1}]$, $[CuLH_{-2}]^{-}$, and $[CuL_2H_{-1}]^{-}$ were taken into account for all four systems, together with the inactive species $[Cu_2L_2H_{-3}]^{-}$. In order to obtain a satisfactory fit for the spectral series, $[CuLH]^{2+}$ was also included for the *c*/*t*ACHC-F−copper(II) systems; for F-*t*ACHC, $[CuL_2]$ too had to be taken into consideration, and the spectrum of $[CuL_2H_{-1}]^{-}$ had to be described as the superimposition of two components, indicating two isomers for the latter species. (Figure S5 illustrates the systematic worsening of the spectral fit for the Cu(II)-F-*t*ACHC system, when $[CuL_2]$ or one of the isomers of $[CuL_2H_{-1}]^{-}$ is omitted.) In the latter case, we should note, however, that the difference in the fit for the one-component model or the various possible two-component models is too small to fully justify the accepted model; here, the best two-component description was supported by chemical considerations, as follows. When only one species was assumed, its EPR parameters differed significantly from those obtained for the corresponding complexes of the other ligands shown in Table 3, i.e., g_o was much lower, and the lines were significantly broader. In contrast, when the chosen two-component model was applied, one of the component spectra was reminiscent of the corresponding results obtained for the other systems with respect to the g_o and A_o values and the line width parameters. With the accepted models, the spectral fit was good in all the spectral series (Figure 4, and Figures S2−S4), and the isotropic EPR parameters (Table 3) and the derived component spectra were comparable to each other (Figure S6).

Complex Stabilities and Coordination Modes. In agreement with the basicities of the donor groups, significant differences in complexing ability were observed between the C- or N-terminal derivatives of ACHC. The formation of $[CuLH]^{2+}$, in which the only possible coordinating donor is the carboxylate group, could not be detected for those peptides where ACHC is in the C-terminal position, in spite of the deprotonation constants

dx.doi.org/10.1021/ic2016116 | *Inorg. Chem.* 2012, 51, 1386−1399

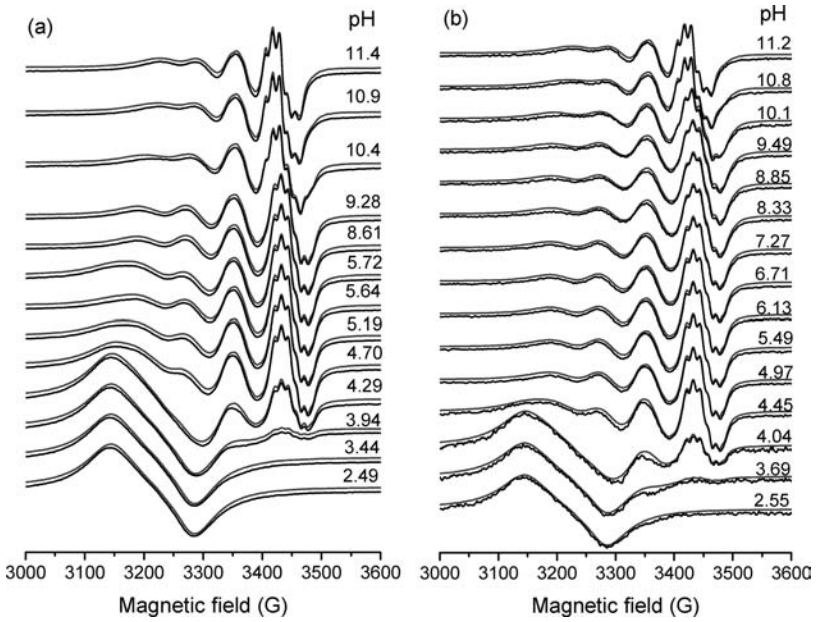

Figure 4. Experimental CW-EPR spectra (black) together with the simulated curves (gray) for the copper(II)−F-*c*ACHC system at 298 K, at (a) T_{Cu} = 3 mM, T_L = 3 mM and (b) T_{Cu} = 1 mM, T_L = 10 mM.

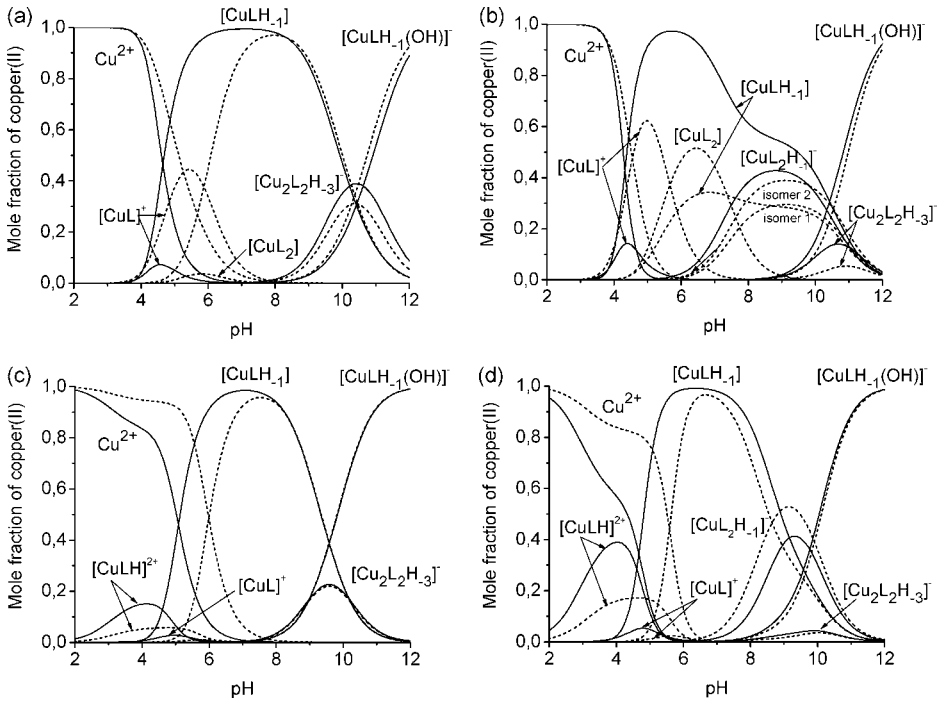

Figure 5. Distribution of the copper(II) complexes formed for the *cis* (solid lines) and *trans* (dotted lines) isomers of ligand F-*c*/*t*ACHC at (a) T_{Cu} = 3 mM, T_L = 3 mM and (b) T_{Cu} = 1 mM, T_L = 10 mM, and for the ligand *c*/*t*ACHC-F at (c) T_{Cu} = 3 mM, T_L = 3 mM and (d) T_{Cu} = 1 mM, T_L = 10 mM.

(less acidic character) of their carboxylate groups (Table 2). For *c*/*t*ACHC-F, the g_o values obtained for $[CuLH]^{2+}$ were slightly less than those for the aqua complex (Table 3), indicating a slightly stronger ligand field, in accordance with the coordination of the carboxylate group.

The maximum concentration of $[CuL]^+$ for β-Ala-Gly was earlier found to be larger than that for Gly-β-Ala, and this was explained by the formation of a more stable six-membered chelate ring by the $\{NH_2,CO\}$ groups for the former ligand, relative to the five-membered chelate for the latter one.[38] In our case, however, $[CuL]^+$ was found to be more stable for F-*c*/*t*ACHC than for *c*/*t*ACHC-F (Figure 5a, c). For the explanation of this difference, the effect of the cyclohexane ring also has to be taken into account. In the case of the ACHC derivatives, the higher stability of the six-membered chelate ring may be suppressed by the lower flexibility of the cyclohexane ring bearing the donor groups, and the more rigid ligand structure may lead to a less stable complex. Higher g_o values for

dx.doi.org/10.1021/ic2016116 | *Inorg. Chem.* 2012, 51, 1386−1399

Table 3. Isotropic EPR Parameters for the Copper(II) Complexes of F-*c*/*t*ACHC and *c*/*t*ACHC-F[a]

complex	F-*c*ACHC			F-*t*ACHC			*c*ACHC-F			*t*ACHC-F		
	g_o	$\lvert A^{Cu}_o\rvert$/ MHz	$\lvert A^{N}_o\rvert$ /MHz	g_o	$\lvert A^{Cu}_o\rvert$ /MHz	$\lvert A^{N}_o\rvert$ /MHz	g_o	$\lvert A^{Cu}_o\rvert$ /MHz	$\lvert A^{N}_o\rvert$ /MHz	g_o	$\lvert A^{Cu}_o\rvert$ /MHz	$\lvert A^{N}_o\rvert$ /MHz
Cu^{2+}	2.1924(1)	104.6(3)		2.1921(1)	103.4(3)		2.1952(1)	104.2(3)		2.1956(1)	106.3(3)	
$[CuLH]^{2+}$							2.1872(1)	117.2(9)		2.1803(2)	108.3(8)	
$[CuL]^{+}$	2.1546(2)	157.7(3)	18.1(3)	2.1576(1)	158.2(3)	28(1)[b]	2.1638(1)	160(1)	18.2(6)	2.1629(4)	126.2(3)	18.2(6)
$[CuLH_{-1}]$	2.1122(1)	224.7(3)	42.0(3)	2.1196(1)	204.4(3)	38.1(3)	2.1177(1)	224.4(3)	44.5(3)	2.1156(1)	228.9(3)	45.6(1)
			33.4(3)			33.2(6)			32.6(3)			33.2(1)
$[CuLH_{-1}(OH)]^{-}$	2.1068(1)	172.8(3)	37.7(3)	2.1143(1)	153.3(3)	34.0(3)	2.1099(1)	214.4(3)	36.9(3)	2.1079(1)	217.1(3)	39.5(3)
			33.6(3)			32.6(3)			36.9(3)			38.3(3)
$[CuL_2]$				2.1142(4)	149(1)	39(1)						
						39(1)						
$[Cu_2H_{-1}]^{-}$												
isomer 1	2.1016(2)	208.2(8)	37(1)	2.1003(4)	225(1)	39(1)	2.1050(1)	243(1)	30(2)	2.1039(1)	248.2(8)	35(2)
			27(1)			25(1)			27(3)			26(1)
isomer 2				2.0901(5)	137(3)	40.0(3)						
						35.5(3)						

[a]The numbers in parentheses represent 3σ for the fit, with σ the standard error, corresponding to a confidence level of 99.7% as explained in ref 18. Note that these values underestimate the real experimental error, since equally good fits with similar statistical agreement can in principle be obtained for other sets of parameters. As explained in the text, chemical considerations were taken into account to decide between the different sets, whereby care was taken to simulate the spectra with a minimal of parameters, *i.e.* complexes. [b]An equally good fit could be optained with a lower A^N_o value but larger line width.

the complexes of *c*/*t*ACHC-F support a weaker ligand field, in accordance with the lower stability of these species (Table 3). The coordination modes proposed for the various complexes are shown in Figure S7.

Loss of the peptide NH proton and the formation of $[CuLH_{-1}]$ with $\{NH_2,N^-,COO^-\}$ coordination are favorable for all dipeptides, and this complex is predominant near the physiological pH. The well-resolved isotropic EPR spectra reveal the hyperfine interaction with two nonequivalent nitrogens (Figure 4 and Figures S2 − S4), which can be characterized with nearly identical coupling constants for the various ligands (Table 3, $[CuLH_{-1}]$). The deprotonation p*K* values for the amide groups of the *c*ACHC derivatives (Table 2) are significantly lower than those for *β*-Ala-Gly or Gly-*β*-Ala, and they are independent of the C- or N-terminal position of the *β*-amino-acid moiety (4.78 for the *β*-Ala derivatives, and 3.84 and 3.85 for F-*c*ACHC and *c*ACHC-F, respectively). However, a considerable difference was found between the *cis*- and *trans*-ACHC derivatives: the *trans* isomers are deprotonated at higher pH (pK_{amide} = 5.87 for F-*t*ACHC and 4.32 for *t*ACHC-F). The concentration distribution curves also illustrate that the complexes $[CuLH_{-1}]$ of the *trans* isomers are less favored: their predominant pH ranges are much narrower (Figure 5). As the basicities of the donor groups for the *cis*/*trans* pairs were found to differ only slightly, this significant difference in complexation ability cannot be attributed solely to electrostatic effects. The isotropic EPR parameters (Table 3) were found to be very similar for $[CuLH_{-1}]$ of *c*ACHC-F and *t*ACHC-F (Δg_o = 0.002, ΔA_o = 4.5 MHz), in accordance with the slight difference in their stability. At the same time, a higher g_o and a lower A_o indicate a significantly weaker ligand field for F-*t*ACHC, forming a significantly less stable complex than that for F-*c*ACHC (Δg_o = 0.0074, ΔA_o = 20.3 MHz).

The loss of a proton from a coordinated water molecule, leading to the formation of $[CuLH_{-1}(OH)]^-$, occurs at significantly lower pH for *c*/*t*ACHC-F than for F-*c*/*t*ACHC. It is accompanied by a small but significant decrease in g_o for all ligands, relative to $[CuLH_{-1}]$, indicating that the hydroxido group occupies an equatorial position in the coordination sphere. The copper hyperfine coupling of $[CuLH_{-1}(OH)]^-$ is decreased considerably for the F-*c*/*t*ACHC ligands and slightly for *c*/*t*ACHC-F, as compared with the coupling constants for the corresponding complexes $[CuLH_{-1}]$ (Table 3), indicating a considerable rhombic distortion. Simultaneously, the nitrogen superhyperfine splitting becomes better resolved for all ligands (Figure S6), and the difference between the nitrogen coupling constants is much smaller (Table 3). The reason for this will be explained on the basis of the low-temperature EPR parameters discussed below.

The formation of the EPR-silent complex $[Cu_2L_2H_{-3}]^-$ in alkaline solution was deduced from the decrease in the double integral of the isotropic EPR spectra. A similar species has been identified for several other dipeptides.[41−43] The EPR inactivity suggests strong antiferromagnetic coupling between the two copper(II) ions, supporting the formation of a hydroxide bridge between the two $[CuLH_{-1}]$ moieties as the most probable structure for this complex (Figure S7).

The complex $[CuL_2]$ with 2{NH_2,CO} coordination could be detected only in the F-*t*ACHC—copper(II) system, where the amide deprotonation was observed to have a significantly higher p*K* (lower stability of $[CuLH_{-1}]$). In the other three systems, the higher stability of the tridentate coordination in $[CuLH_{-1}]$ suppresses the formation of the above species.

dx.doi.org/10.1021/ic2016116 | Inorg. Chem. 2012, 51, 1386−1399

For $[CuL_2H_{-1}]^-$ with glycylglycine and other dipeptides built up from α-amino acids, $\{NH_2,N^-,COO^-\}$ coordination for the ligand LH_{-1} and $\{NH_{2,eq},CO_{ax}\}$ coordination for L have been suggested.[41,44] The stronger ligand field was manifested in a decrease in g_o and an increase in A_o as compared with $[CuLH_{-1}]$. Similar changes in parameters were observed for the complexes $[CuL_2H_{-1}]^-$ of *c*/*t*ACHC-F (Table 3), supporting also the above coordination mode for this case. For F-*c*ACHC and isomer 1 of F-*t*ACHC, the decrease in g_o was accompanied by a significant decrease in A_o, which is typical when rhombic distortion occurs in a complex; the change is attributed to a reduced Fermi contact term as a consequence of 3d−4s orbital mixing.[45] This rhombic distortion may be explained by the smaller size of the chelate ring formed by $\{NH_{2,eq},CO_{ax}\}$, which is only a five-membered one for F-*c*/*t*ACHC (in contrast with the six-membered one for *c*/*t*ACHC-F). For F-*t*ACHC, another isomer of $[CuL_2H_{-1}]^-$ was also identified (isomer 2). The appearance of this species can again be explained by the moderate stability of $[CuLH_{-1}]$, which allows the formation of complexes through exclusion of the carboxylate group from the equatorial coordination. For isomer 2, the equatorial coordination $\{NH_2,N^-\}\{NH_2,CO\}$ is suggested (Figure S7), i.e. the bidentate binding is probable for both ligands. In this respect, the structure of this isomer molecule is reminiscent of that of $[CuL_2]$. The similarities in coordination mode are supported by the analogous strong relaxation, manifested in broad EPR lines for both species (Figure S6).

We thus conclude that the observed differences between the complexation abilities of *cis* and *trans* stereoisomers cannot be explained solely on the basis of deprotonation p*K* or isotropic EPR data. In order to elucidate these differences, a more advanced CW and pulsed EPR analysis of the predominant *mono*complexes of the stereoisomers was performed. Low-temperature CW and ESE-detected EPR experiments were used to determine the **g** and copper hyperfine tensors, while ELDOR-detected NMR and HYSCORE target at obtaining the hyperfine and nuclear quadrupole tensors of the surrounding magnetic nuclei. The spectral interpretations in the next sections are corroborated by DFT computations.

Low-Temperature X-Band CW-EPR and W-Band ESE-Detected EPR Experiments. The X-band CW-EPR curves at 77 K of the predominant complexes $[CuLH_{-1}]$ and $[CuLH_{-1}(OH)]^-$ demonstrate a well-resolved hyperfine structure in the region of $g \approx g_\perp$, corresponding to two equatorial nitrogen donor atoms and copper nuclei (Figure 6). A good spectral fit could be obtained only by assuming rhombic **g**-, $\mathbf{A}^{Cu}$-, and $\mathbf{A}^{N}$-tensors. The anisotropic EPR parameters are collected in Table 4, while the agreement between the experimental and simulated spectra is illustrated in Figures 3 and 6. The signs of the hyperfine principal values were chosen on the basis of the DFT results (see later) and the experimental isotropic hyperfine values (Table 3), taking into account that $A_o = (A_x + A_y + A_z)/3$. Figure 7 shows the coordination modes proposed for the complexes $[CuLH_{-1}]$ and the principal directions of the **g**-tensor, together with the directions of the largest nitrogen hyperfine and quadrupole couplings obtained from spectrum simulations (see also the following sections).

The most striking difference between the frozen solution spectra of $[CuLH_{-1}]$ for *c*/*t*ACHC-F and F-*c*/*t*ACHC is the stronger rhombic character of the **g**-tensor for the former ligands (Table 4). The same trend was found in the W-band ESE-detected EPR spectra, which could be simulated well with the EPR parameters obtained from the X-band EPR spectra. In

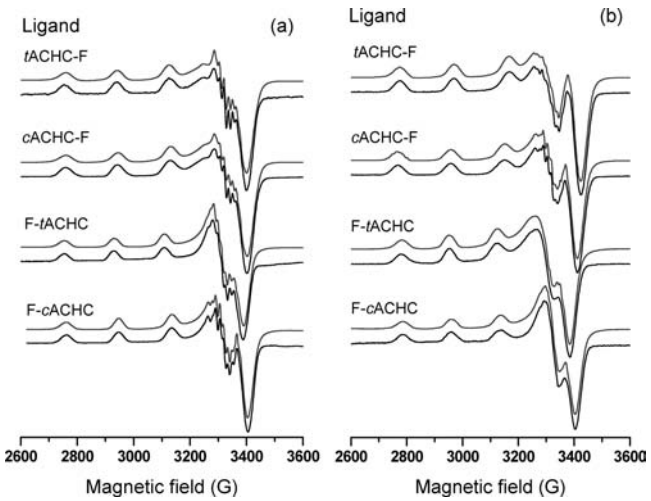

Figure 6. Experimental (black) and calculated (gray) CW-EPR spectra at 77 K (a) at pH = 7.5, where $[CuLH_{-1}]$ predominates, and (b) at pH = 12, where $[CuLH_{-1}(OH)]^-$ predominates.

the W-band spectra, the broader lines in the $g \approx g_{x,y}$ region support the higher *g*-anisotropy for *c*/*t*ACHC-F (Figure S8). In accordance with the isotropic EPR curves, the frozen solution spectra for the *cis* and *trans* isomers of the ACHC-F complexes are quite similar, while the *cis*−*trans* pair of F-ACHC complexes exhibit significant differences, particularly in the $g \approx g_{x,y}$ region (Figure 6a). The species $[CuLH_{-1}]$ for F-*t*ACHC has a significantly larger g_z and smaller A_z than those of the other three complexes. This indicates a considerably weaker ligand field for this complex, in agreement with the differences in the isotropic EPR parameters (Table 3) and its small formation constant (Table 2). The destabilization of $[CuLH_{-1}]$ for F-*t*ACHC can be attributed to a steric effect. To obtain more detailed information on the structure, pulsed-EPR experiments are needed to measure the nitrogen hyperfine couplings, since the broad parallel lines in the CW-EPR spectrum do not allow a reliable determination of the nitrogen couplings in the *z* direction. Moreover, it is not possible to assign the related *x* and *y* principal values of the nitrogen coupling tensors on the basis of CW-EPR alone. Therefore, the nitrogen hyperfine and quadrupole tensors were determined by W-band ELDOR-detected NMR (specified below).

For the mixed hydroxido complexes ($[CuLH_{-1}(OH)]^-$), g_z (and g_x) were considerably lower than those for $[CuLH_{-1}]$, reflecting the stronger ligand field induced by OH^-, which replaces an equatorial H_2O molecule. In the event of effective D_{4h} symmetry, decreasing g_z values are accompanied by increasing A_z values,[45] and this was observed for *c*/*t*ACHC-F. However, for the F-*c*/*t*ACHC complexes, the opposite variation of the copper hyperfine coupling was found (similarly as for the isotropic EPR parameters), and the nitrogen-related splitting was not observed in the $g \approx g_{x,y}$ region (Figure 6b). The smallest A_z value was again that for F-*t*ACHC. For the mixed hydroxido complexes of diglycine[41] and glycyl-L-histidine,[44] a similarly lower A_z was previously observed and explained by the rhombic distortion induced by the repulsion of the two neighboring, negatively charged OH^- and COO^- groups. This may also be the case in F-*c*/*t*ACHC, enhanced by the fact that the six-membered chelate ring forces the carboxylate group closer to the OH^-. For diglycine[41] and glycyl-L-histidine,[44] it was also observed that the two nonequivalent nitrogen couplings in $[CuLH_{-1}]$ could not be distinguished in the mixed

dx.doi.org/10.1021/ic2016116 | *Inorg. Chem.* 2012, 51, 1386−1399

Table 4. Comparison of g and A^{Cu} Principal Values of the Complexes $[CuLH_{-1}]$ and $[CuLH_{-1}(OH)]^-$ for the Ligands F-*c*/*t*ACHC and *c*/*t*ACHC-F, Determined through CW-EPR Measurements at 77 K and by DFT Methods

complex	g_x	g_y	g_z	A_x/MHz[a]	A_y/MHz[a]	A_z/MHz	$A_{o,calc}$/MHz[b]
$[CuLH_{-1}]$							
CW-EPR Experiment[c]							
F-*c*ACHC	2.038	2.053	2.237	−69	−58	−574	−233.6
F-*t*ACHC	2.040	2.057	2.252	−54	−62	−547	−221.1
*c*ACHC-F	2.031	2.059	2.237	−64	−101	−562	−242.3
*t*ACHC-F	2.031	2.059	2.240	−65	−106	−560	−243.8
DFT Calculations							
F-*c*ACHC, conf 1	2.039	2.056	2.154	−21	33	−582	−189.8
F-*t*ACHC	2.038	2.063	2.160	−26	65	−557	−172.5
*c*ACHC-F, conf 1	2.036	2.065	2.156	−38	80	−559	−172.2
*t*ACHC-F	2.034	2.068	2.156	−44	98	−555	−167.2
$[CuLH_{-1}(OH)]^-$							
CW-EPR Experiment[c]							
F-*c*ACHC	2.036	2.049	2.233	71	−41	−533	−167.8
F-*t*ACHC	2.035	2.052	2.226	90	−54	−518	−160.8
*c*ACHC-F	2.034	2.051	2.225	−74	71	−581	−194.7
*t*ACHC-F	2.032	2.051	2.215	−103	53	−589	−213.1

[a]For CW-EPR, the signs of the experimental values were derived from a comparison of $A_{o,calc}$ with the experimental A_o values in Table 3. [b]Isotropic coupling calculated via the equation $A_o = (A_x + A_y + A_z)/3$. [c]The experimental errors were ±0.001 for g_x and g_y, ±0.0005 for A_z, ±2 MHz for A_x and A_y, and ±1 MHz for A_z.

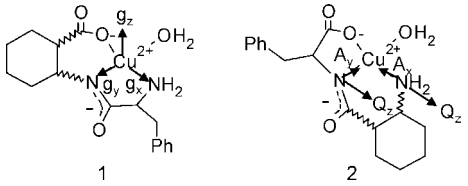

Figure 7. Equatorial coordination around copper(II) in the complex $[CuLH_{-1}]$ of **1**: F-*c*/*t*ACHC and **2**: *c*/*t*ACHC-F. Selected orientations for the complexes $[CuLH_{-1}]$ are also shown: the **g**-tensor orientation in structure **1**, and the orientations of the largest nitrogen hyperfine and quadrupole couplings in structure **2**.

hydroxido complex, while a much better resolved nitrogen hyperfine structure was detected in the isotropic EPR spectra. The same tendency can be observed in the isotropic nitrogen hyperfine couplings (Table 3) for the complexes of the ACHC dipeptides too. The exact equality of the nitrogen couplings would suggest a lower degree of covalency of the nitrogen−copper(II) σ-bond for the amide and a higher degree for the amino nitrogen. The analysis of the well-resolved nitrogen bands in the frozen solution EPR spectra of $[CuLH_{-1}(OH)]$ for *c*/*t*ACHC-F (Figure 6b), however, did not support the equivalency of the donor nitrogens. The anisotropic nitrogen couplings could be determined with high accuracy, and the isotropic nitrogen coupling constants were calculated from the anisotropic parameters (Table 4). These data do not differ strongly from those of the corresponding $[CuLH_{-1}]$ complexes (e.g., for F-*c*ACHC, values of $A_o^N{}_{,amide}$ = 42.0 MHz and $A_o^N{}_{,amino}$ = 33.4 MHz were measured for $[CuLH_{-1}]$, and of $A_o^N{}_{,amide}$ = 38.3 MHz and $A_o^N{}_{,amino}$ = 31.0 MHz for $[CuLH_{-1}(OH)]$). At the same time, the anisotropy of the nitrogen couplings was significantly decreased, especially for the amide nitrogen (e.g., for F-*c*ACHC, the measured couplings A_x, A_y, and A_z are 39, 44, and 32 MHz, respectively, for $[CuLH_{-1}]$, and 40, 41, and 44 MHz for $[CuLH_{-1}(OH)]^-$). These data suggest that the less covalent copper−N σ-bonds of the amide nitrogen are compensated by more covalent π-bonds in the mixed hydroxido complex, as assumed previously for diglycine on the basis of the isotropic nitrogen coupling constants.[41] Our data furnish evidence that the equivalence of the nitrogen couplings in solution is only apparent; this is caused by the limitation of the spectral resolution in the broad isotropic EPR spectra.

W-Band ELDOR-Detected NMR Experiments. A series of orientation-selected ELDOR-detected NMR spectra and the corresponding simulation of the ^{14}N contributions to the spectra are depicted in Figure 8 for the Cu(II) complexes of the

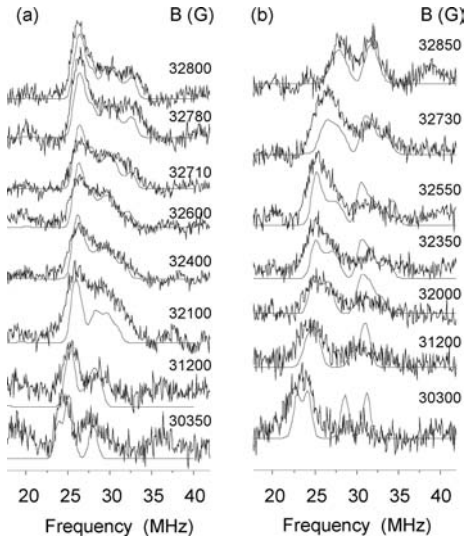

Figure 8. W-band ELDOR-detected NMR spectra at 6 K for the complex $[CuLH_{-1}]$ of (a) F-*c*ACHC and (b) *c*ACHC-F, recorded at different observer positions: black lines, measured spectra; gray lines, simulated curves.

cis ligands (F-*c*ACHC and *c*ACHC-F). For the corresponding *cis*−*trans* ligand pairs, these spectra were found to be very similar (Figures S9 and S10). The simulation of the ELDOR-detected NMR spectra revealed that the two larger principal values (A_x^N and A_y^N) relate to each other, most probably originating from the amide nitrogen (as supported by DFT results, discussed below). The smaller A_x^N and A_y^N values can

dx.doi.org/10.1021/ic2016116 | Inorg. Chem. 2012, 51, 1386−1399

Table 5. Principal Values of the ^{14}N Hyperfine and Quadrupole Coupling Tensors Determined by Different Experimental and Theoretical Methods for the Complexes $[CuLH_{-1}]$ and $[CuLH_{-1}(OH)]^-$ of the Different Dipeptides under Study[a]

		N_{amide}						NH_2					
	method	A_x/MHz	A_y/MHz	A_z/MHz	(e^2qQ/h)/MHz	η[b]	$A_{o,calc}$[c]/MHz	A_x/MHz	A_y/MHz	A_z/MHz	(e^2qQ/h)/MHz	η[b]	$A_{o,calc}$[c]/MHz
$[CuLH_{-1}]$													
L = F-*c*ACHC	CW-EPR[d]	39	44	32			38.3	32	33	28			31.0
	ELDOR[e]	40	42	34	3.4	0.4	38.6	35	32	30	(−)1.0	0.4	32.3
	DFT	41	60	42	2.4	0.6	47.7	41	29	29	−2.8	0.3	33.0
L = F-*t*ACHC	CW-EPR[d]	41	44	37			40.7	34	26	23			27.7
	ELDOR[e]	39	40	32	3.4	0.4	40.7	34	31	28	(−)1.0	0.4	31.0
	DFT	40	58	38	2.4	0.6	45.1	41	28	28	−2.8	0.3	32.3
L = *c*ACHC-F	CW-EPR[d]	45	48	40			44.3	36	29	28			31.0
	ELDOR[e]	43	45	41	3.0	0.4	43.0	38	30	28	(−)1.0	0.4	32.0
	DFT	42	60	43	2.6	0.84	48.3	38	26	25	−2.6	0.1	29.7
L = *t*ACHC-F	CW-EPR[d]	45	49	41			45.0	38	26	28			30.7
	ELDOR[e]	45	45	43	3.0	0.4	44.3	38	31	28	(−)1.0	0.4	32.3
	DFT	49	66	50	2.6	0.84	55.0	40	27	27	−2.6	0.1	31.3
$[CuLH_{-1}(OH)]^-$													
L = F-*c*ACHC	CW-EPR[d]	40	41	44			41.7	28	28	22			26.0
L = F-*t*ACHC	CW-EPR[d]	41	41	43			41.7	25	29	25			26.3
L = *c*ACHC-F	CW-EPR[d]	44	43	48			45.0	33	34	33			33.3
L = *t*ACHC-F	CW-EPR[d]	44	44	45			44.3	28	29	29			28.7

[a]The *x*, *y*, *z* directions refer to the **g**-tensor orientations. [b]The nuclear quadrupole principal values, $[Q_x, Q_y, Q_z]$, are expressed as $[-K(1-\eta), -K(1+\eta), 2K]$, where $K = e^2qQ/(4I(2I-1)h)$ is the quadrupole coupling constant for ^{14}N ($I = 1$), and $\eta = (Q_x - Q_y)/Q_z$ is the asymmetry parameter. Q is the nuclear quadrupole moment, and eq is the electric field gradient. The Euler angles of the quadrupole tensors were $\alpha = 90°$, $\beta = 90°$, $\gamma = 0°$ for the amide and $\alpha = 0°$, $\beta = 90°$, $\gamma = 0°$ for the amino nitrogen. [c]Isotropic coupling calculated via the equation $A_o = (A_x + A_y + A_z)/3$. [d]The experimental errors were ±1 MHz for A_x and A_y and ±2 MHz for A_z. [e]The experimental errors were ±0.5 MHz for A_x, A_y, and A_z, ±0.2 MHz for e^2qQ/h, and ±0.1 for η.

be assigned to the amino nitrogen (Table 5). These measurements allowed determination of the ^{14}N hyperfine coupling constant in the *z* direction with higher accuracy. The larger value was again assigned to the amide nitrogen. For the complexes $[CuLH_{-1}(OH)]^-$, the ELDOR-detected NMR spectra could unfortunately not be measured, since copper hydroxide precipitated at 6 K and pH ∼ 11.

DFT Computation of EPR Parameters. To facilitate the interpretation of the differences observed in the EPR data, supporting DFT computations were performed. The theoretical calculation of EPR data of copper(II) complexes can be problematic in some respects: the deviation in *g* from the free-electron value is usually underestimated, and calculation of the copper hyperfine couplings (particularly the A_x and A_y values) is difficult, because of the similar magnitudes of the Fermi contact and spin-dipolar couplings and the contributions from the spin−orbit interaction, with varying sign.[46] At the same time, the geometries and the differences in EPR parameters predicted by DFT methods can indicate reliable trends. Furthermore, the hyperfine values of the surrounding ligand nuclei tend to be better reproduced by the computations. Our goal was to apply a consistent DFT approach for calculations on the stereoisomers of copper(II) complexes and to compare the tendencies in the calculated EPR parameters for the optimized geometries with the data determined experimentally. The geometry of certain selected complexes was tested (Tables 4 and 5; Tables S1 and S2). First, the coordination numbers of such copper(II) complexes were examined by varying the number of possible axial water molecules from zero to two. The complex with two axially coordinated water molecules was found not to be stable: a five-coordinated complex was obtained after geometry optimization in each case. The computed principal values of the **g**- and $\mathbf{A}^{Cu}$-tensors for the complex with axial coordination of one water were rather close to the experimental rhombic values, while zero axial water molecules led to quasi-axial symmetry for the **g**-tensor (Table S1). The five-coordinated model was therefore chosen to optimize the complex geometries, in accordance with the fact that crystalline copper(II) peptide complexes usually exhibit distorted square-pyramidal geometry.[47] In the next step, tests on the up or down position of the axial water molecule resulted in very similar EPR parameters. The impact of the phenyl group position on the single point energy and EPR parameters was additionally tested, by calculating the above data with the phenyl group rotated by 120° or 240° around the $C_\alpha-CH_2$ single bond. No significant differences were detected (Table S1).

Although the absolute values of numerous parameters differed considerably from the corresponding experimental data (*e.g.*, g_z and copper A_x and A_y values),[46] similar trends were observed for the experimental and calculated data, indicating that the theoretically computed EPR data reflect the geometrical differences well (Table 4). The larger g_z ($\Delta g_{z,exp} = 0.015$) and smaller A_z ($\Delta A_{z,exp} = 27$ MHz) values obtained from the CW-EPR measurements for the complexes $[CuLH_{-1}]$ with the F-*c*/*t*ACHC ligand pairs are in good agreement with the DFT results ($\Delta g_{z,calc} = 0.006$, $\Delta A_{z,calc} = 25$ MHz), indicating that the lower stability of $[CuLH_{-1}]$ for F-*t*ACHC is due to the weaker ligand field present in this species.

The experimental EPR data obtained for the complexes $[CuLH_{-1}]$ of the *c*/*t*ACHC-F ligand pair are in good accord with the theoretically calculated EPR parameters (Table 4). The assignment of the higher ^{14}N hyperfine coupling observed in the W-band ELDOR-detected NMR experiments is supported by the computed nitrogen hyperfine data: larger hyperfine values were obtained for the amide than for the

dx.doi.org/10.1021/ic2016116 | Inorg. Chem. 2012, 51, 1386−1399

amino nitrogens. (It should be noted, however, that the computations significantly overestimated the isotropic hyperfine value and the anisotropy of these couplings.) At the same time, reasonable data were found for the nitrogen quadrupole values, and the orientation of the largest quadrupole couplings (Q_z) agreed well with experimental findings. Earlier ^{14}N nuclear quadrupole resonance studies on diglycine[48] revealed that the quadrupole coupling for the amide, ($(e^2qQ)/h$ = 3.030, η = 0.410) is larger than that for the amino nitrogen ($(e^2qQ)/h$ = 1.280, η = 0.410), and the largest value (Q_z) is oriented parallel to the lone pair of the nitrogen. These values were used as initial data for the simulation of the ELDOR-detected NMR spectra, but for the complexes [CuLH$_{-1}$] the orientation of the largest quadrupole value was found to lie in the *xy* plane for both nitrogens: perpendicular to the amide nitrogen−copper(II) bond for the amide nitrogen, and parallel to the amino nitrogen−copper(II) bond for the amino nitrogen (Figure 7). These orientations are supported by the current DFT calculations. A similar orientation of the largest quadrupole coupling as in the case of the amide nitrogen in ACHC complexes has been found both experimentally and theoretically for the imidazole nitrogens in hemin complexes.[49,50]

The nitrogen coupling constants obtained through use of the various experimental and theoretical methods are compared in Table 5. Significant differences exist between the complexes of the ligands containing the ACHC moiety in the C- or N-terminal positions: the isotropic coupling constants obtained for the amide nitrogen were larger for *c*/*t*ACHC-F than for F-*c*/*t*ACHC, and this difference was also manifested in the theoretically calculated data. The differences were particularly large for the principal values in the *z* direction, indicating a more covalent out-of-plane π-bond between the nitrogen and copper(II) for [CuLH$_{-1}$] in the case of *c*/*t*ACHC-F. The A_x^N values for the amino nitrogen, which has its principal axis along the nitrogen−copper(II) bond, were also larger for *c*/*t*ACHC-F than for F-*c*/*t*ACHC. This can be explained by the stronger basicity of the amino groups measured for the free ligands. Overall, it may be stated that the findings deduced from the experimental data are in good agreement with the results of DFT computations collected in Table 5.

The above-mentioned EPR data show that the coordination sphere of copper(II) is very similar for the *cis* and *trans* pairs. Only the F-*c*/*t*ACHC case seems to differ. Moreover, the DFT calculations do not indicate a significant destabilization of the [CuLH$_{-1}$] complex structure for the *trans* isomers. From these results, we can exclude that the lower stability constants of the *trans* isomers, detected in solution, originate from a markedly destabilized structure. We therefore presume that the enhanced stability of the copper(II) complexes of the *cis* isomers in solution must be explained by the fact that, in the *cis* case, both cyclohexane conformers (conformers 1 and 2 in Table 1) appear to coordinate to the copper(II) ion in solution, contrasting the *trans* isomer case, for which only the equatorial−equatorial conformer is able to bind. At low temperature, however, only the thermodynamically most stable conformer may be prevailing. In order to confirm this assumption, the conformation of the cyclohexane ring in the complexes [CuLH$_{-1}$] has been probed by measuring the proton hyperfine couplings of the ligands by ^{1}H-HYSCORE experiments at 10 K.

X-Band ^{1}H-HYSCORE Experiments versus DFT. Two sets of HYSCORE measurements were performed in order to detect the ^{1}H hyperfine couplings. First, aqueous solutions of samples containing the predominant complex [CuLH$_{-1}$] were measured. In this case, the large proton couplings of the amino and the equatorially and axially coordinated water protons led to maximal ^{1}H hyperfine couplings of the order of 15−20 MHz being obtained (Figure S12). Even though these HYSCORE signals are rich in proton peaks, the evaluation is generally very complicated and offers little information about the structure of the ligand coordinating to the copper(II) ion. To eliminate these signals, the HYSCORE measurements were performed in deuterated water, so as to detect merely the nonexchangeable (ligand) proton signals originating from the C$_\alpha$-H proton of the phenylalanine (F) part and the cyclohexane ring protons (Figure 9). In this case, the largest measured ^{1}H couplings were in the 2−5 MHz range, and combination peaks between the ^{1}H and ^{2}H nuclear frequencies appeared, centered at 12.3 and 16.9 MHz (at 334.0 mT). In the simulation of the HYSCORE spectra depicted in Figure 9, only the basic ^{1}H frequencies were taken into account. The two largest proton couplings obtained by DFT calculations were used as starting values for the simulations. Since the dipolar coupling between the protons and the unpaired electron was found to be larger than the Fermi contact term, the largest proton couplings were directed approximately toward the copper(II) ion (Figure 10). The simulated HYSCORE spectra are compared with the experimental ones in Figure 9 for three different observer positions for the complex [CuLH$_{-1}$] of the two *cis* ligand isomers, F-*c*ACHC and *c*ACHC-F. The HYSCORE spectra of the *trans* isomers resemble the corresponding *cis* cases (Figure S11). The ^{1}H hyperfine coupling data obtained from the simulation are compared with the computed data in Table 6. The structures of the complexes [CuLH$_{-1}$] and the orientations of the two largest proton couplings are shown in Figure 10.

First, we simulated the HYSCORE spectra of the *trans* isomers, where only the conformer with both 1,2-groups equatorial in the cyclohexane ring can coordinate to the copper(II) ion. In this case, the C$_\alpha$−H and ring proton positions are fixed around the copper(II) ion, and the ^{1}H HYSCORE spectrum can be well described by changing the calculated DFT data only slightly. For the *cis* isomers, however, two different chair conformers with different proton orientations and hyperfine couplings can coordinate. For the case when the ring proton lies next to a nitrogen in the *xy* plane, a very large proton coupling is predicted by DFT, with a large Fermi contact contribution: a maximal principal hyperfine value of 16.3 MHz for conformer 1 of F-*c*ACHC and of 13.2 MHz for conformer 2 of *c*ACHC-F (Table 6). Since no such coupling has been observed for either of the two HYSCORE sets, the complexes of the other conformers, *i.e.* conformer 2 for F-*c*ACHC and conformer 1 for *c*ACHC-F, seem to dominate under the measuring conditions (10 K). It has, however, been shown earlier that some HYSCORE peaks of weakly modulating nuclei may be suppressed by the strong modulation of a second nucleus (e.g., ^{2}H).[51] To exclude that such a suppression effect lies at the bottom of the current observations, HYSCORE simulations were performed using the DFT-computed values for conformers 1 and 2 of the F-*c*ACHC case in combination with a typical ^{2}H coupling (Supporting Information, Figure S13). From this it is obvious that the stronger proton coupling of conformer 1, if present, should be observable under the used experimental conditions.

The HYSCORE spectra of the *c*ACHC-F complex could be well described by starting from the calculated proton hyperfine couplings and orientations of conformer 1 (see Table 6). These results agree with the DFT computation of the free ligand,

dx.doi.org/10.1021/ic2016116 | *Inorg. Chem.* 2012, 51, 1386−1399

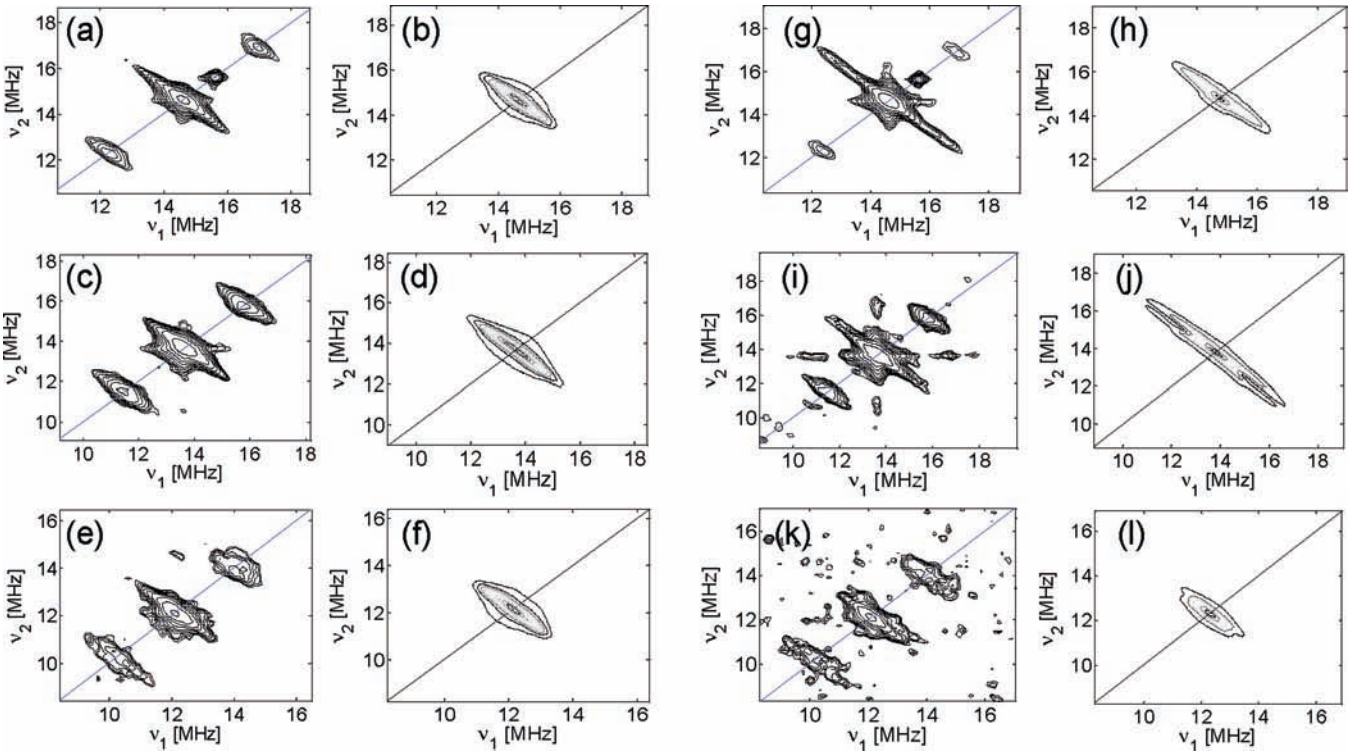

Figure 9. Experimental X-band proton HYSCORE spectra taken at 10 K for the complex [CuLH$_{-1}$] (in 60% vol/vol D_2O/H_2O) of (a, c, e) F-*c*ACHC and (g, i, k) *c*ACHC-F. Experimental and simulated pairs are shown in (a, b) and (g, h) for the observer positions $g \approx g_x$ (B_0 = 334.0 mT), (c, d) and (i, j) for the intermediate observer position (B_0 = 320.0 mT), and (e, f) and (k, l) for the observer position $g = g_z$, $M_I = {}^3/_2$(B_0 = 284.0 mT).

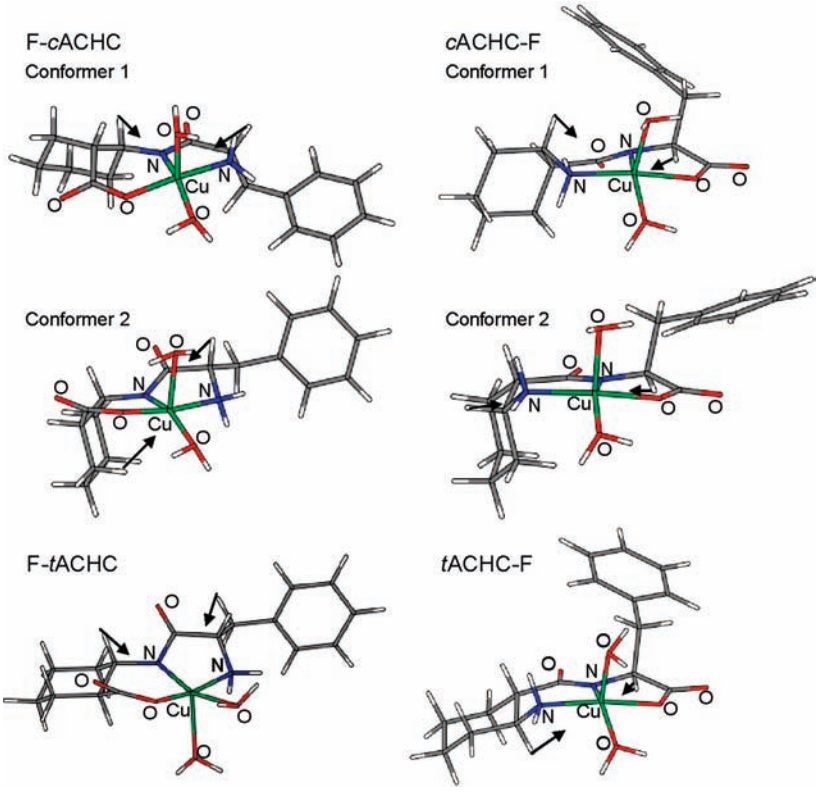

Figure 10. Structures of the complex [CuLH$_{-1}$] for the ligands *c*/*t*ACHC-F and F-*c*/*t*ACHC and the directions of the A^H_x axis (shown in Table 6), obtained from the DFT calculations.

which predicted the predominance of conformer 1 (79.5%) over conformer 2 (20.5%) at 77 K (Table 1). For F-*c*ACHC, the DFT conformer analysis likewise predicted the predominance of conformer 1; surprisingly, however, the combined HYSCORE/DFT results suggested the opposite situation, with the preferential formation of conformer 2 formed at low temperature.

dx.doi.org/10.1021/ic2016116 | *Inorg. Chem.* 2012, 51, 1386−1399

Table 6. Comparison of the Principal Values A^H and Orientations Obtained by ^{1}H HYSCORE Spectrum Simulation and DFT Calculations for the Complexes [CuLH$_{-1}$] of Ligands F-*c*/*t*ACHC and *c*/*t*ACHC-F

		C_α-H				C_{ring}-H[a]			
ligand		A_x/MHz	A_y/MHz	A_z/MHz	Euler angles, $\alpha\ \beta\ \gamma$ (deg)	A_x/MHz	A_y/MHz	A_z/MHz	Euler angles, $\alpha\ \beta\ \gamma$ (deg)
F-*c*ACHC	HYSCORE[b]	3.8	−2.9	−2.9	−25 30 0	4.0	−2.0	−2.0	35 50 0
	DFT for conf 1	7.1	3.2	2.2	−29 11 0	16.3	11.4	10.8	75 16 0
	DFT for conf 2	3.8	−2.9	−2.2	−25 30 0	5.6	−2.9	−2.5	45 60 0
F-*t*ACHC	HYSCORE[b]	3.7	−2.9	−2.2	−28 30 0	7.7	2.1	2.4	67 15 0
	DFT	3.7	−2.9	−2.2	−33 20 0	7.7	2.1	2.4	67 15 0
*c*ACHC-F	HYSCORE[b]	7.0	2.7	1.8	−60 13 0	7.3	−3.0	−3.0	35 40 0
	DFT for conf 1	7.6	2.7	1.7	−57 13 0	5.3	−2.0	−1.0	30 30 0
	DFT for conf 2	7.9	2.9	2.0	−57 13 0	13.2	9.4	8.7	18 10 0
*t*ACHC-F	HYSCORE[b]	7.0	2.7	1.8	−70 12 0	7.8	−3.0	−3.0	35 34 0
	DFT	7.8	2.7	1.8	−64 12 0	7.2	−0.6	0.1	30 44 0

[a]Different ring protons with the largest coupling values were selected. [b]The experimental errors were ±0.1 MHz for A_x, ±0.3 MHz for A_y and A_z, and ±2° for Euler angles.

In our opinion, this result supports the assumption that the conformation distribution changes significantly upon complexation, relative to the situation for the free ligand, and thus the copper(II) complexes of both conformers may exist, and the proportions of the conformers even may undergo a drastic change. For the F-*c*ACHC complex, this change may be explained by the more strained ring formed in conformer 1, with a $C_{carb}-O_{carb}-Cu$ angle of 127°, whereas in conformer 2 this angle is 122° and, hence, appreciably closer to the optimal 120° of a six-membered chelate ring. Though such a conformational diversity could not be revealed directly by CW EPR, because of the large similarity in *g* and copper hyperfine parameters, the current HYSCORE observation indicates the significantly higher stability of the *cis* stereoisomer complexes, compared to the *trans* ligands, detected in the solution equilibrium study. Since the higher stabilities of the *cis* complexes were manifested only in the formation constants, and no significant stabilization was detected in the structures of their complexes [CuLH$_{-1}$] at low temperature (especially for the *c*/*t*ACHC-F ligand pairs), the most probable reason for the enhanced stability is the existence of different conformation isomers (not only chair but also twist and boat conformers, with higher energies) in liquid solutions at room temperature. For the *trans* stereoisomers, this isomerization is limited to the complexes formed with equatorial−equatorial ring positions of the coordinated donor groups.

CONCLUSIONS

The copper(II) binding properties of alicyclic *β*-amino acid dipeptides with phenylalanine (F-*c*/*t*ACHC and *c*/*t*ACHC-F) have been investigated through the use of various EPR techniques and DFT calculations. To facilitate the spectral interpretations, the stereochemistry and the deprotonation constants of the free ligands have also been determined.

The complexation abilities of the stereoisomeric pairs F-*c*/*t*ACHC and *c*/*t*ACHC-F display the following similarities: (a) the EPR-active complexes, $[Cu(aqua)]^{2+}$, $[CuL]^{+}$, [CuLH$_{-1}$], [CuLH$_{-1}$(OH)]$^{-}$, and [CuL$_2$H$_{-1}$]$^{-}$, and the inactive species [Cu$_2$L$_2$H$_{-3}$]$^{-}$ can be identified in all systems, and (b) the complex [CuLH$_{-1}$] formed by tridentate {NH$_2$,N^{-},COO^{-}} coordination of the ligand predominates near the physiological pH. The main differences between the dipeptides with the 2-ACHC moiety in the N- or the C-terminal position are that (a) $[CuLH]^{2+}$ can also be formed in the former case and (b) the complexes [CuLH$_{-1}$] and [CuLH$_{-1}$(OH)]$^{-}$ are more stable for *c*/*t*ACHC-F dipeptides than for the corresponding stereoisomers of F-*c*/*t*ACHC, which can be ascribed to the higher basicity of their amino groups.

Our results revealed that all possible conformation isomers of 1,2-disubstituted cyclohexanes should be taken into account in their complex equilibria with metal ions, and the most stable conformer of the free ligand is not always that which leads to the most stable conformation in the complex. The considerably higher stabilities of the *cis* isomer complexes relative to those of the corresponding complexes of the *trans* isomers, for instance, can be explained by the presence of such conformation isomers in solution: for the *trans* ligands, the chair conformer of the cyclohexane ring containing both donor groups in axial positions cannot bind to the metal ion in a bidentate manner, which strongly limits the number of possible conformer complexes. In contrast, for the *cis* stereoisomers, both conformers have an equatorial−axial position of the donor groups and can thus bind the metal ion, and this is accompanied by enhanced stability in the equilibrium systems in solution.

The low-temperature CW-EPR study demonstrated that the lowest stability of [CuLH$_{-1}$] for F-*t*ACHC is associated with the weakest ligand field in the series of analogous complexes. In this system, the low stability of [CuLH$_{-1}$] allows the formation of [CuL$_2$] and two isomers for [CuL$_2$H$_{-1}$]$^{-}$. The nitrogen hyperfine tensors for [CuLH$_{-1}$] and [CuLH$_{-1}$(OH)]$^{-}$ furnish spectral evidence of the change in covalency of the metal−ligand bonds: the in-plane *σ*-bond becomes less covalent, while the out-of-plane *π*-bond of the deprotonated amide nitrogen becomes more covalent upon formation of the mixed hydroxido complex. Comparison of theoretically calculated ^{1}H couplings with those obtained from HYSCORE measurements revealed the conformation of the cyclohexane ring in the most stable complex [CuLH$_{-1}$]. It was found that this does not always involve the most stable conformer of the free ligand.

ASSOCIATED CONTENT

Supporting Information

Full reference of ref 21; structures of F-*t*ACHC stereoisomers and copper(II) complexes; simulated CW-EPR spectral series of F-*t*ACHC− and *c*/*t*ACHC-F−copper(II) systems; component isotropic EPR spectra of F-*c*/*t*ACHC and *c*/*t*ACHC-F complexes; W-band ESE-detected EPR spectra for [CuLH$_{-1}$] of F-*c*/*t*ACHC and *c*/*t*ACHC-F; full W-band ELDOR-detected NMR spectrum for the complex [CuLH$_{-1}$] of F-*c*ACHC; W-band ELDOR-detected NMR and X-band HYSCORE spectra of F-*t*ACHC and *t*ACHC-F [CuLH$_{-1}$] complexes together with simulations; X-band HYSCORE spectra of *t*ACHC-F [CuLH$_{-1}$] in aqueous solution; anisotropic EPR

dx.doi.org/10.1021/ic2016116 | Inorg. Chem. 2012, 51, 1386−1399

parameters obtained by DFT calculations for different coordination arrangements; structural data of the optimized [$CuLH_{-1}$] geometries. This material is available free of charge via the Internet at http://pubs.acs.org.

AUTHOR INFORMATION

Corresponding Author

*Telephone: +36-1-4381131. Fax: +36-1-4381143. E-mail address: nagyn@chemres.hu.

ACKNOWLEDGMENTS

The financial support of the Hungarian Scientific Research Fund (OTKA, Grant F67581), the Fund for Scientific Research-Flanders (FWO, Grant G.0468.03), and the COST Action P15 program is gratefully acknowledged.

REFERENCES

(1) Fülöp, F. *Chem. Rev.* **2001**, *101*, 2181−2204.
(2) Ohki, H.; Inamoto, Y.; Kawabata, K.; Kamimura, T.; Sakane, K. *J. Antibiot.* **1991**, *44*, 546.
(3) Hintermann, T.; Seebach, D. *Chimia* **1997**, *51*, 244−248.
(4) Abele, S.; Seebach, D. *Eur. J. Org. Chem.* **2000**, 1−15.
(5) Dado, G. P.; Gellman, S. H. *J. Am. Chem. Soc.* **1994**, *116* (3), 1054−1062.
(6) Porter, E. A.; Wang, X.; Lee, H. S.; Weisblum, B.; Gellman, S. H. *Nature* **2000**, *404*, 565.
(7) Fülöp, F.; Martinek, T. A.; Tóth, G. K. *Chem. Soc. Rev.* **2006**, *35* (4), 323−334.
(8) Martinek, T. A.; Mandity, I. M.; Fülöp, L.; Tóth, G. K.; Vass, E.; Hollósi, M.; Forró, E.; Fülöp, F. *J. Am. Chem. Soc.* **2006**, *128* (41), 13539−13544.
(9) Barchi, J. J.; Huang, X. L.; Appella, D. H.; Christianson, L. A.; Durell, S. R.; Gellman, S. H. *J. Am. Chem. Soc.* **2000**, *122* (12), 2711−2718.
(10) Dutot, L.; Gaucher, A.; Elkassimi, K.; Drapeau, J.; Wakselman, M.; Mazaleyrat, J. P.; Peggion, C.; Formaggio, F.; Toniolo, C. *Chem.—Eur. J.* **2008**, *14* (10), 3154−3163.
(11) Kritzer, J. A.; Lear, J. D.; Hodsdon, M. E.; Schepartz, A. *J. Am. Chem. Soc.* **2004**, *126*, 9468−9469.
(12) Schmitt, M. A.; Weisblum, B.; Gellman, S. H. *J. Am. Chem. Soc.* **2007**, *129*, 417.
(13) Karlsson, A. J.; Pomerantz, W. L.; Neilsen, J. K.; Gellman, S. H.; Palecek, S. P. *ACS Chem. Biol.* **2009**, *4*, 567−579.
(14) Schmitt, M. A.; Weisblum, B.; Gellman, S. H.; Palecek, S. P. *J. Am. Chem. Soc.* **2006**, *128*, 12630.
(15) Mondal, J.; Zhu, X.; Cui, Q.; Yethiraj, A. *J. Phys. Chem. B* **2010**, *114*, 13585−13592.
(16) Rossi, F.; Lelai, G.; Seebach, D. *Helv. Chim. Acta* **2003**, *86* (7), 2653−2661.
(17) Hyyrylainen, A. R. M.; Pakarinen, J. M. H.; Fülöp, F.; Vainiotalo, P. *J. Am. Soc. Mass Spectrom.* **2009**, *20*, 34−41.
(18) Tamura, S. Y.; Goldman, E. A.; Brunck, T. K.; Ripka, W. C.; Semple, J. E. *Bioorg. Med. Chem. Lett.* **1997**, *7*, 331−339.
(19) Harmat, N. J. S.; Di Bugno, C.; Criscuoli, M.; Giorgi, R.; Lippi, A.; Martinelli, A.; Monti, S.; Subissi, A. *Bioorg. Med. Chem. Lett.* **1998**, *8*, 1249−1254.
(20) Zékány, L.; Nagypál, I.; Peintler, G. *PSEQUAD for Chemical Equilibria*; Technical Software Distributors: Baltimore, MD, 1991.
(21) Schosseler, P.; Wacker, Th.; Schweiger, A. *Chem. Phys. Lett.* **1994**, *224*, 319.
(22) Höfer, P.; Grupp, A.; Nebenführ, H.; Mehring, M. *Chem. Phys. Lett.* **1986**, *132*, 279.
(23) Rockenbauer, A.; Szabó-Plánka, T.; Árkosi, Zs.; Korecz, L. *J. Am. Chem. Soc.* **2001**, *123*, 7646−7654.
(24) Rockenbauer, A.; Korecz, L. *Appl. Magn. Reson.* **1996**, *10*, 29−43.
(25) Stoll, S.; Schweiger, A. *J. Magn. Reson.* **2006**, *178* (1), 42−55.
(26) Frisch, M. J.; et al.; *Gaussian 09*, Revision A.1; Gaussian, Inc.: Wallingford, CT, 2009.
(27) Neese, F. *ORCA—an ab initio, density functional and semi empirical program package*, Version 2.6; University of Bonn: Bonn, Germany, 2008.
(28) Neese, F. *J. Chem. Phys.* **2001**, *115*, 11080−11096.
(29) Neese, F. *J. Phys. Chem. A* **2001**, *105*, 4290−4299.
(30) Neese, F. *J. Chem. Phys.* **2003**, *118*, 3939−3948.
(31) Neese, F. *J. Chem. Phys.* **2005**, *122*, 034107.
(32) Sinnecker, S.; Fajendran, A.; Klamt, A.; Diedenhof, M.; Neese, F. *J. Phys. Chem. A* **2006**, *110*, 2235.
(33) Schaefer, A.; Horn, H.; Ahlrichs, R. *Chem. Phys. Lett.* **1995**, *240*, 283.
(34) Stephens, P. J.; Devlin, F. J.; Chabalowsky, C. F.; Frisch, M. J. *J. Phys. Chem.* **1994**, *98*, 11623−11627.
(35) The Ahlrichs polarization functions were obtained from the Turbo-Mole basis set library under ftp.chemie.uni-karlsruhe.de/pub/basen 2p functions from: Wachters, A. J. H. *Chem. Phys.* **1970**, *52*, 1033 plus one f-function from the TurboMole library.
(36) Barone, C. In *Recent Advances in Density Functional Methods*; Chong, D. P., Ed.; World Scientific Publishing Co.: Singapore, 1996; p 287.
(37) Beckett, C. W; Pitzer, K. S.; Spitzer, R. *J. Am. Chem. Soc.* **1947**, *69*, 2488.
(38) Sóvágó, I.; Sanna, D.; Dessí, A.; Várnagy, K.; Micera, G. *J. Inorg. Biochem.* **1996**, *63*, 99−117.
(39) Sóvágó, I.; Radomska, B.; Schön, I.; Nyéki, O. *Polyhedron* **1990**, *9*, 825−830.
(40) Inomata, Y.; Yamaguchi, T.; Tomita, A.; Yamada, D.; Howell, F. S. *J. Inorg. Chem.* **2005**, *99*, 1611−1618.
(41) Nagy, N. V.; Szabó-Plánka, T.; Rockenbauer, A.; Peintler, G.; Nagypál, I.; Korecz, L. *J. Am. Chem. Soc.* **2003**, *125*, 5227−5235.
(42) Szabó-Plánka, T.; Árkosi, Zs.; Rockenbauer, A.; Korecz, L. *Polyhedron* **2001**, *20* (9−10), 995−1003.
(43) Szabó-Plánka, T.; Nagy, N. V.; Rockenbauer, A.; Korecz, L. *Inorg. Chem.* **2002**, *41*, 3483−3490.
(44) Szabó-Plánka, T.; Nagy, N.; Rockenbauer, A.; Korecz, L. *Polyhedron* **2000**, *19*, 2049−2057.
(45) Rockenbauer, A. *J. Magn. Reson.* **1979**, *35*, 429−438.
(46) Neese, F. *J. Biol. Inorg. Chem.* **2006**, *11*, 702−711.
(47) Ryvkin, F.; Greenaway, F. T. *Bioinorg. Chem. Appl.* **2010**, DOI: 10.1155/2010/724210.
(48) Rabbani, A. R.; Edmonds, D. T.; Gosling, P. *J. Magn. Reson.* **1987**, *72*, 230−237.
(49) Jiang, F. S.; Zuberi, T. M.; Cornelius, J. B.; Clarkson, R. B.; Gennis, R. B.; Belford, R. L. *J. Am. Chem. Soc.* **1993**, *115*, 10293−10299.
(50) Behzadi, H.; van der Spoel, D.; Esrafili, M. D.; Parsafar, G. A.; Hadipour, N. L. *Biophys. Chem.* **2008**, *134* (3), 200−206.
(51) Stoll, S.; Calle, C.; Mitrikas, G.; Schweiger, A. *J. Magn. Reson.* **2005**, *177*, 93−101.